FREQUENCY-DOMAIN MMSE TURBO EQUALIZATION OF MULTILEVEL CODED QAM – CONVERGENCE IN REAL FIELDS

Kimmo Kansanen, Tad Matsumoto

University of Oulu
Oulu, Finland

Christian Schneider, Reiner Thomä

Ilmenau Technical University
Ilmenau, Germany

Abstract— **Convergence properties of frequency domain turbo equalization with multilevel bit-interleaved coded modulation (MLBICM) and bit-interleaved coded modulation (BICM) are studied in measured quasi-static fading channels by the means of semi-analytical convergence analysis. Spatial channel parameters are matched to the reached mutual information on a per-measurement basis and trends in the behavior of the equalizer are obtained, when the channel characteristics, in terms of transmit and receive side azimuth spreads, change. Robust convergence of frequency-domain turbo equalization combined with multilevel BICM is demonstrated through the convergence analysis. Three channel codes are evaluated in the measurement-based simulation showing the effects of outer code selection.**

I. Introduction

Turbo equalization is one of the most promising techniques to implement well-performing equalizers without requiring excessive computational complexity. In this paper we concentrate on the evaluation of the frequency-domain soft interference canceling minimum mean-square error (MMSE) turbo equalization in multiple-input-multiple-output (MIMO) scenarios. The algorithm in question has been presented e.g. in [1] and its convergence properties in multipath fading channels analyzed in [2], where it was shown how the spatial selectivity of the channel influences the effective output signal-to-noise ratio (SNR) of the equalizer and the convergence properties of the equalizer. Reduced spatial selectivity reduces the effective SNR and the required SNR for successful convergence is increased.

In [3] MLBICM and BICM were compared in real fields with the time-domain MMSE turbo equalizer receiver by simulations. In this paper we study these modulations in the real fields using the semi-analytical convergence analysis presented in [2] and channel measurement data. Estimated spatial channel parameters are compared with the convergence behavior of the equalizer. Furthermore, different channel codes are evaluated for both MLBICM and BICM for convergence behavior. It is shown how averaging the mutual information in BICM de-mapping incurs a loss compared to MLBICM and results in significantly poorer convergence for turbo equalization.

This paper is organized as follows. The considered system is described in Section II. The principles of the applied semi-analytical turbo equalizer convergence analysis are described in Section III, whereas a complete description can be found in [2]. The channel measurement scenario and data is presented in Section IV followed by numerical results in Section V. The paper concludes with a summary.

II. Considered system

The system employs two transmit and two receive antennas. The transmission is (multilevel-) bit-interleaved coded modulation (BICM) with 16-QAM modulation, and each transmit antenna sends an independently encoded and modulated symbol stream. The transmission is assumed to contain a cyclic prefix which enables efficient frequency-domain processing at the receiver. The MLBICM transmission is depicted in Fig. 1, with the decoding of one transmit antenna's signal depicted at the receiver. The MLBICM transmission is constructed by the superposition of two Gray-mapped QPSK modulations, referred to as "layers" in the sequel, with an amplitude weighting to produce a symmetric 16-QAM modulation. Layer-1 refers to the component determining the 16-QAM modulation quadrant, and Layer-2 refers to the component determining the constellation point within the quadrant. The weighting allocates the transmitted power in $4/1$ ratio to the layers. Due to the difference in distance properties of the layers, they provide unequal error protection (UEP) to transmitted bits. However, this property also serves to enhance the convergence properties of the modulation when combined with turbo equalization.

The channel is assumed to be a frequency-selective MIMO channel and to remain static over the transmitted frame. Due to the cyclic transmission and the static channel assumption, a simple filter having one coefficient per receive antenna per frequency bin can be applied for equalization at the receiver [2].

The superpositioned modulation can be decoded without explicit symbol-to-bit de-mapping at the receiver [4]. Both layers can use a single MMSE filter followed by layer-wise post-combining with prior information. Symbol de-mapping is replaced by the likelihood computation for binary symbols. The channel decoder provides soft extrinsic information of

978-3-8007-2909-8/05/$20.00 ©2005 IEEE

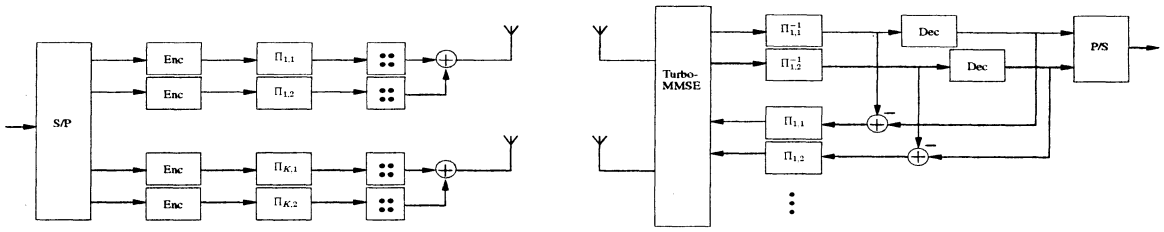

Fig. 1. MLBICM transmission and reception.

encoded bits based on the equalizer output likelihoods. This soft information is used in interference cancellation at the next iteration in the form of soft symbol estimates.

The BICM transmission utilizes Gray-mapped 16-QAM, which is symbol-to-bit de-mapped at the receiver to obtain bit-level likelihood information for the decoder. The channel decoder accepts these as input and computes extrinsic likelihoods for the encoded bits, which are then used to compute a soft symbol estimate for each transmitted symbol. Both coded modulations are assumed to use the same channel code, including both MLBICM layers.

III. Convergence Analysis by Semi-analytical EXIT charts

The semi-analytical convergence analysis for one turbo iteration contains four phases. Firstly, the expected residual interference variance based on the mutual information of the decoder feedback is computed as

$$\bar{\lambda}_k = \mathrm{E}\left\{\mathrm{E}\left\{|\mathrm{s}_k|^2\right\} - |\hat{\mathrm{s}}_k|^2\right\}, \quad (1)$$

where the first expectation is taken over the a-priori probability distribution of the transmitted symbols s_k of transmit antenna k, and the second over the transmitted sequence. The notation $\hat{(\cdot)}$ denotes an MMSE estimate. The likelihood feedback used in forming $\hat{\mathrm{s}}$ is assumed to have Gaussian density. The residual variance is a function of the feedback mutual information and the mapping and for any fixed mapping it can be pre-computed.

Secondly, the effective SNR of the equivalent Gaussian channel assumed at the output of the equalizer is computed for each transmit antenna k as

$$\Lambda_k = \frac{\mu_k}{1-\mu_k}, \quad (2)$$

where

$$\mu_k = \bar{\gamma}_k \left(1 + \bar{\gamma}_k \delta_k\right)^{-1}, \quad (3)$$

which is computed using the definitions

$$\delta_k = 1 - \bar{\lambda}_k \quad (4)$$

$$\bar{\gamma}_k = N^{-1}\mathbf{tr}\left\{\mathbf{\Xi}_k^{\mathrm{H}}\left(\sigma_0^2\mathbf{I} + \sum_{k=1}^{K}\bar{\lambda}_k\mathbf{\Xi}_k\mathbf{\Xi}_k^{\mathrm{H}}\right)^{-1}\mathbf{\Xi}_k\right\} \quad (5)$$

In the above, $\mathbf{\Xi}_k$ denotes the single-input multiple-output channel matrix of transmit antenna k, and N is the length of the transmitted sequence.

Thirdly, the average mutual information of the de-mapped bits, assuming an equivalent Gaussian channel output of the equalizer, is computed as

$$I_{e,k} = C_B\left(\mu_{k,a}, B\right) - \frac{1}{2M}\sum_{j=1}^{M}\sum_{k=0}^{1} C_{B_k^j}\left(\mu_{k,a}, B\right), \quad (6)$$

where $C_{B_k^j}$ is the constellation constrained capacity (CCC) [5] of the jth sub-constellation consisting of the points where the bit j takes the value k. The CCC of a constellation in an AWGN channel with variance $\mu_{k,a}\left(1-\mu_{k,a}\right)/2$ per dimension given by

$$C_B\left(\mu_{k,a}, B\right) = M - 2^{-M}\sum_{i=1}^{M}$$

$$\mathrm{E}\left\{\log_2\sum_{j=1}^{M}\exp\left(-\frac{\left|\mu_{k,a}\left(b_i - b_j\right) + v\right|^2 - |v|^2}{\mu_{k,a}\left(1-\mu_{k,a}\right)}\right)\right\}. \quad (7)$$

The sub-constellations are defined by the mapping rule assumed and the value of $C_{B_k^j}$ can be computed with (7) by setting $M \rightarrow M-1$ and defining $b_{[i,j]}$ for the sub-constellation. The expectation in (7) is taken over the two-dimensional Gaussian distribution of the zero-mean complex noise variable v. The average mutual information function is mapping-specific, fixed, and can be pre-computed and approximated with a functional approximation [2], [6].

The first three phases of the analysisi form the computation of the equalizer extrinsic information transfer (EXIT) function using the knowledge of the prior information, the channel state and the receiver noise level. Finally, the decoder extrinsic and a-posteriori information based on the input mutual information is computed. The decoder EXIT function is code- and decoder algorithm -specific and can be pre-computed.

The MLBICM analysis is based on the fact that for the two coded streams per antenna, indexed by $m \in [1,2]$, the propagation channel is identical. The layer-wise value of (5) for the two layers have the relation of $\bar{\gamma}_{k,1} = 4\bar{\gamma}_{k,2}$, and the residual interference given by (1) becomes the sum over the layers. The de-mapper average mutual information

is computed for each m using (7) assuming a Gray-coded QPSK constellation. Effectively the convergence analysis tracks the mutual information of two de-mapper outputs per transmit antenna, compared to one for BICM. The post-cancelation linear MMSE equalizer itself behaves identically for the two coded modulations. Initially, it is assumed the prior information is not available and the effective SNR of the linear frequency-domain MMSE filter is computed. The four analysis phases are repeated until a stopping condition examining the change in mutual information between consecutive iterations is met. The a-posteriori information of the coded bits corresponding to the fixed point reached by the iterations is then found and used as an estimate of the information of the decoded bits. When the input mutual information is above 0.7 this provides an accurate result.

The state of the MIMO channel determines the spatial separability of the two transmissions [2] and the effective SNR at the equalizer output as indicated by (5). Due to the random nature of the channel, the convergence of the equalizer is essentially random. Using the semi-analytical method described above the distribution of the reached fixed point over a given set of channel realizations can be evaluated.

IV. Channel Measurements

The measurements were conducted at the campus of the Ilmenau University of Technology using a 5.2 GHz carrier frequency and a channel sounding system bandwidth of 120 MHz. Two transmit and two receive antennas were selected from the measurement equipment and 108 snapshots of the corresponding channel impulse response data was used in the numerical evaluations. The approximate element spacings for the selected elements were 2 wavelengths at the transmitter and 4 wavelengths at the receiver side. The measured channel impulse responses (CIR) were concatenated with root-raised-cosine filters having 25MHz bandwidth and 0.2 roll-off, resulting in a band-limited channel consistent with a 20Msps transmission rate. The channel responses were normalized to have unity mean energy between the selected transmit and receive antenna pairs, effectively imposing an assumption of perfect short-term received power control. This allows the study of spatial effects without the influence of short-term fading on the link performance. The received SNR is defined as

$$SNR = \frac{E_b N_R}{N_0 N_T}, \tag{8}$$

where N_R is the number of receive antennas, N_T is the number of transmit antennas, E_b is the transmitted energy per bit, and N_0 is the receiver noise power.

During the measurement of the first 15 snapshots the transmitter is immobile, after which it is moved. During the first 55 snapshots the line-of-sight (LOS) is obstructed by a metal container. From snapshot 56 onwards a LOS is present between the transmitter and the receiver. Using a super-resolution path parameter estimation technique [7], the spatial propagation conditions throughout the measurement track can be identified. A detailed insight into the spatio-temporal multipath structure of the measurement area can be found in [8]. The transmitter and receiver side azimuthal spreads are reported in Fig. 2 and 3. The largest rms azimuthal spread at the transmitter side can be found within the first 15 snapshots, where the transmitter was not moving. This indicates a multipath-rich environment due to the non line-of-sight (NLOS) propagation. During the measurement of snapshots between 16 and 55 the transmitter was moving along the measurement track. During this section the propagation is still NLOS, but exhibiting medium transmitter and receiver azimuthal spreads. For the rest of the track the propagation is LOS and the azimuthal spreads are significantly lower compared to the NLOS sections. Receive side azimuthal spread is much smaller than the transmit side due to the 120° beamwidth of the ULA elements used.

V. Numerical Evaluations

With the convergence analysis technique outlined in Section III we evaluate the required SNR to reach a certain mutual information target at the channel decoder a-posteriori output (here chosen to be 0.999). The considered channel code is the rate-$1/2$ convolutional code with generators $(561, 753)_8$. Fig. 2 reports the required SNR for BICM in each snapshot along the measurement track. The dependence between the azimuthal spreads and the required SNR is easily verified. A comparable result for MLBICM is reported in Fig. 3, where the two layers are reported separately. Layer-2 exhibits an SNR threshold (approx. 9dB) below which it does not reach the target.

It is notable that in snapshots where the SNR requirement is higher than the threshold, both layers converge at the same SNR. This result shows when it is possible to further optimize the code design or -selection for MLBICM either for

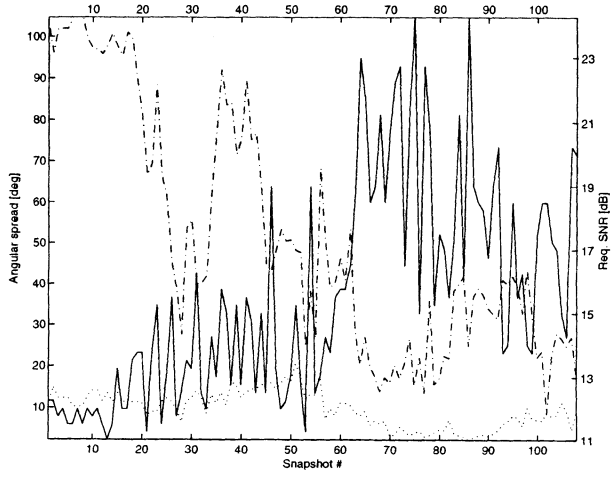

Fig. 2. Required SNR (solid) for BICM, TX and RX Azimuth spread (dash-dot, dot).

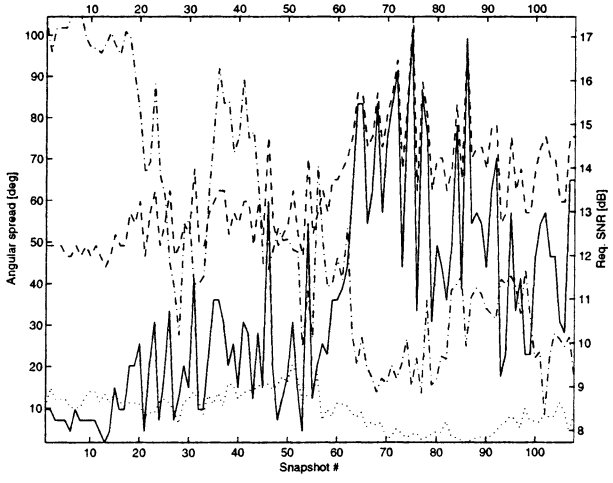

Fig. 3. Required SNR (Layer-1: solid, Layer-2: dashed) for MLBICM, TX and RX Azimuth spread (dash-dot, dot).

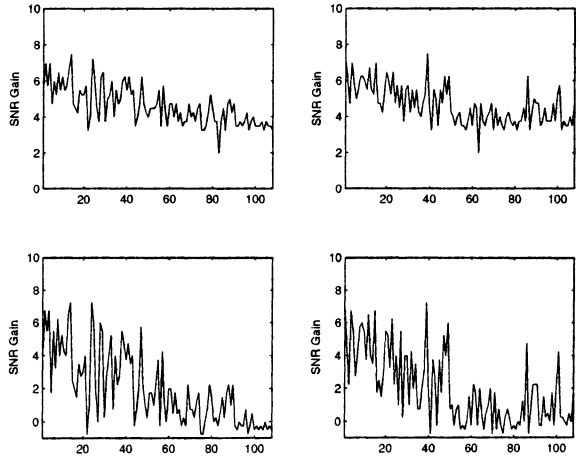

Fig. 4. SNR Gain of MLBICM (top: Layer-1, bottom: Layer-2 over BICM with increasing TX (left) and RX (right) azimuth spread.

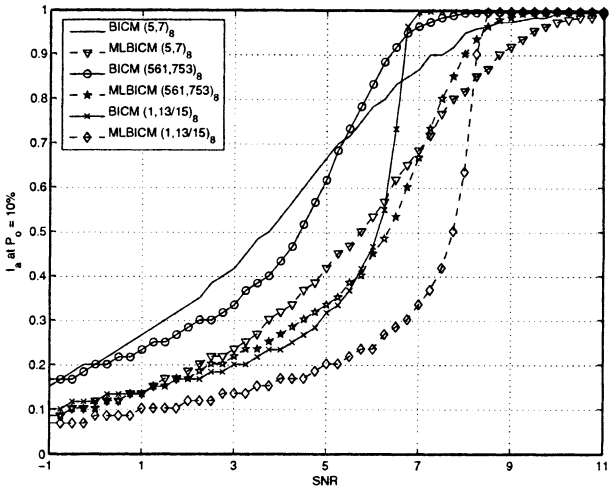

Fig. 5. 10% Outage mutual information at the GAD bound with different channel codes.

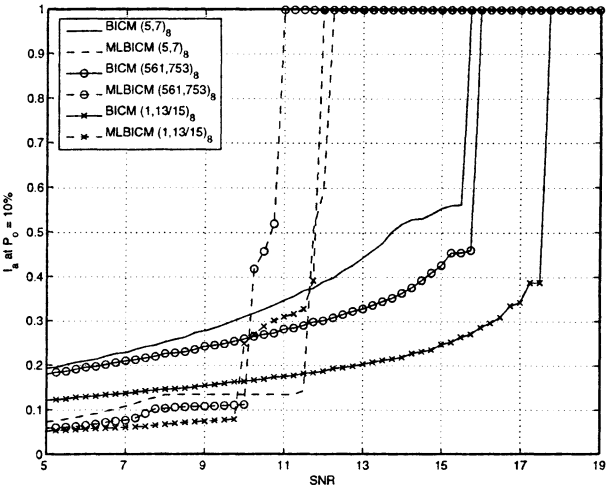

Fig. 6. 10% Outage mutual information with different channel codes.

increased throughput or decreased required SNR. A decrease of code rate will enable convergence with a lower SNR [9]. Optimally both layers should converge at the same SNR, since otherwise power is wasted bringing Layer-2 to the desired operation point. Fig. 3 indicates we can trade (decrease) Layer-2 code rate for Layer-1 rate in high spatial spread environments and achieve a lower required SNR. This results does not, however, prove the optimality of the unbalanced design in the low-spread environments, where the design is convergence-limited and dependent on successful Layer-1 decoding. Any puncturing of the Layer-1 code would lead to an increased required SNR for Layer-1 and, thus, the whole link in these cases. In these scenarios the additional SNR is required to reach the target, or alternatively transmission rate must be decreased. The difference in required SNR between BICM and MLBICM can also be evaluated. Fig. 4 reports MLBICM Layer-1 (top row) and Layer-2 (bottom row) gain over BICM. The channel snapshots have been sorted according to increasing TX (left column) and RX (right column) -side azimuthal spread. Layer-1 gain is mainly interesting if the link is used for the transmission of multiple classes of data and UEP is a desired feature of the link. In cases with a single class of data, Layer-2 dominates the link error performance, and is of primary interest. The gain is largest in low azimuthal spread cases and diminishes as the spread increases. MLBICM Layer-2 provides gain over BICM in high-spread cases but has a small loss in the high-spread cases. This result coincides with earlier results [3] indicating a small advantage for BICM in high spatial spread environments. Finally, an evaluation of the differences of

equalizer converge properties when combined with different channel codes is conducted with the measurement data. The mutual information reached in 90% of the snapshots given perfect channel decoder feedback (genie aided detection) is plotted in Fig. 5 as a function of average received SNR for both MLBICM and BICM. The considered channel codes are the rate-$1/2$ convolutional codes with polynomials $(5,7)_8$ and $(561,753)_8$, and the turbo code with constituent polynomials $(1,13/15)_8$, which is punctured to rate-$1/2$. For MLBICM, the average mutual information over layers is reported for consistency with BICM. With all channel codes BICM reaches a higher mutual information than MLBICM with GAD. The outage mutual information based on the true convergence of the equalizer is reported in Fig. 6 and shows the BICM combined with all the considered codes has severe convergence problems in the considered channel scenarios. With MLBICM, the outage mutual information is mainly a demonstration of the Layer-2 SNR threshold whose effect dominates the average mutual information between layers. Interestingly, the MLBICM modulation combines well with a high-memory outer code, while BICM does not.

A fundamental explanation of the convergence behavior of BICM and MLBICM is given in Fig. 7 where the residual interference power resulting from the first equalization and decoding iteration is plotted as a function of the equalizer output equivalent SNR (linear scale) and the early convergence of MLBICM Layer-1 is visibly demonstrated. The BICM characteristic for converting equalizer output SNR into low residual interference at the next iteration is remarkably poorer. It is instructive to consider the differences between the two coded modulations that result in the behavior in Fig. 7. Since the mapping from decoder feedback mutual information is quite similar between Gray mapped QPSK and 16-QAM, the reason must reside elsewhere. One reason for the behavior is the design of BICM: the de-mapper mixes all encoded bits into one stream and effectively averages the bitwise mutual information. In other words, the sub-optimal constellation constrained capacity of BICM 16-QAM limits the transformation of equalizer output SNR into mutual information entering the decoder. Since the extrinsic information transfer (EXIT) characteristic of most channel codes exhibit a threshold effect wrt. the input mutual information, the limitation due to modulation becomes dominant. To support this interpretation, in Fig. 7 it can be seen that the weakest channel code has the smallest difference between BICM and MLBICM convergence characteristic.

VI. Summary

An approach to semi-analytically track the convergence of the frequency-domain MMSE turbo equalizer was presented. The approach was applied to the convergence evaluation of 16-QAM with BICM and MLBICM coding and modulation. Channel measurement data was used to perform the evaluations in the real field and to compare the results with estimated spatial channel parameters. The robustness

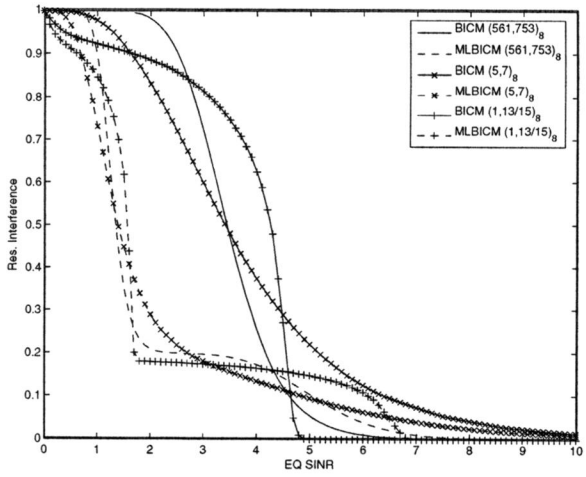

Fig. 7. Equalizer output SNR transformed into residual interference at next iteration.

of MLBICM in channels with varying spatial characteristics was demonstrated with indications on how to further optimise the MLBICM scheme. MLBICM was found to perform well with high-memory convolutional codes, which is the opposite of BICM behavior with outer codes. The mutual information averaging of 16-QAM BICM was found to be the main reason for the poor convergence characteristic of the BICM modulation.

References

[1] M.S. Yee, M. Sandell, and Y. Sun, "Comparison study of single-carrier and multi-carrier modulation using iterative based receiver for MIMO system," in *Proc. IEEE Veh. Technol. Conf.*, Milan, Italy, May 17–19 2004.

[2] K. Kansanen and T. Matsumoto, "Frequency-domain MMSE turbo equalization – convergence in fading channels," *IEEE Trans. Wirel. Commun., submitted*, 2005, also available at http://www.ee.oulu.fi/%7ekmo.

[3] K. Kansanen, C. Schneider, T. Matsumoto, and R. Thomä, "Multilevel coded QAM with MIMO turbo-equalization in broadband single-carrier signaling," *IEEE Trans. Veh. Technol.*, vol. 54, no. 3, pp. 954–966, May 2005.

[4] K. Kansanen and T. Matsumoto, "Turbo equalisation of multilevel coded QAM," in *Proc. IEEE Works. on Sign. Proc. Adv. in Wirel. Comms.*, Rome, Italy, June 15-18 2003.

[5] G. Ungerboeck, "Channel coding with multilevel/phase signals," *IEEE Trans. Inform. Theory*, vol. 28, no. 1, pp. 55–67, Jan. 1982.

[6] F. Brännström, *Convergence Analysis and Design of Multiple Concatenated Codes*, Ph.D. thesis, Chalmers University of Technology, Gothenburg, Sweden, 2004.

[7] R.S. Thomä, D. Hampicke, A. Richter, G. Sommerkorn, and U. Trautwein, "MIMO vector channel sounder measurement for smart antenna system evaluation," *European Trans. Telecommun.*, vol. 12, no. 5, pp. 427–438, Sept. 2001.

[8] C. Schneider, U. Trautwein, T. Matsumoto, and R. Thomä, "Dependency of turbo MIMO equalizer performances on spatial and temporal multipath channel structure - a measurement based evaluation," in *Proc. IEEE Veh. Technol. Conf.*, Jeju, Korea, Apr. 22–25 2003, vol. 1.

[9] A. Ashikhmin, G. Kramer, and S. ten Brink, "Extrinsic information transfer functions: Model and erasure channel properties," *IEEE Trans. Inform. Theory*, vol. 50, no. 11, pp. 2657–2673, Nov. 2004.